Flow structure in the downstream of a square cylinder with different angles of incidence

N. Jamshidi, M. Farhadi, K. Sedighi
Faculty of Mechanical Engineering,
Babol University of Technology, Babol, Iran, P.O. Box 484

ABSTRACT

This paper presents comparisons between flow fields for turbulent flow over square cylinder with two different angles of incidence in free stream at Reynolds number of Re = 3400. The present numerical results were obtained using a two-dimensional finite-volume code which solves governing equations. The pressure field was obtained with well known SIMPLE algorithm. The central difference scheme was employed for the discretization of convection and diffusion terms. The $v2f$ and standard $k-\varepsilon$ model were used for simulation of turbulent flow. Time averaged velocity, root mean square velocities and streamlines in the downstream of square cylinders are presented. A number of quantities such as Strouhal number, drag coefficient and the length of the wake are calculated for the case of angle of incidence $\alpha = 0°, 45°$ with two turbulent models. Strouhal number and the length of the wake are larger for the case of $\alpha = 45°$ because of the sharp corners in it which results in more diffusion of turbulence in the downstream of the cylinder. On the other hand, with comparison of results obtained by $v2f$ and standard $k-\varepsilon$ models with experiment, it is obvious that $v2f$ leads to much more accurate results.

Key words: Turbulent flow; URANS Model; square cylinder; Angle of incidence

1. INTRODUCTION

The flow around slender cylindrical bluff bodies has been the subject of intense research in the past, mostly by experiments but recently also by using numerical simulation. This flow situation is popular not only because of its academic attractiveness but also owing to its related technical problems associated with energy conservation and structural design. This type of flow is of relevance for many practical applications, e.g. vortex flowmeters, buildings, bridges, towers, masts and wires. Under normal circumstances and when these bluff structures are exposed to cross-flow, there is a massive separated region downstream of the body. Owing to wake instabilities, a time-periodic oscillation develops at some critical onset Reynolds number Re_{cr}. This is the Benard von Karman instability. The periodic phenomenon is referred to as vortex shedding, while the antisymmetric wake flow pattern is normally referred to as the Karman vortex street. The oscillating wake rolls up into two staggered rows of vortices with opposite senses of rotation. The frequency of vorticity pairs is a function of velocity, cylinder diameter and Reynolds number [1]. The vortex shedding frequencies and flow configurations are major issues for the design of structures. The flow in the near-wake region behind the cylinder, incorporating the vortex formation region, plays an important role in determining the steady and unsteady forces acting on the body. Periodic vortex shedding patterns and fluctuating velocity fields behind the bluff bodies can cause structural damage as a result of periodic surface loading, acoustic noise and drag forces [1,2].

A considerable amount of experimental data has been gathered for square cylinders (SC) with one side facing the flow. However, experiments on the detailed effects of the angle of incidence are much scarcer. In all these studies the Reynolds numbers are relatively high, ranging from about 500 to 10^5.

Okajima [3] carried out an experimental study of flow past the SC as well as the rectangular cylinder for $70 \leq \mathrm{Re} \leq 2000$ to determine the vortex shedding frequencies. The results showed that there was an abrupt change in Strouhal number when the aspect ratio of the cylinder was reduced to the range 2–3. Strouhal numbers for the SC with an increasing angle of incidence from 0 to 45 were examined using a hot-wire probe in a closed circuit wind-tunnel for Re = 10,000 by Obasaju [4]. LDV measurements were conducted for flow past the SC in a water tunnel for Re = 14,000 and Re = 21,400 [5,6]. Durao et al. [5] separated the periodic and random components of velocity fluctuations around the SC.

The experiment results of Lyn et al. [6] showed a relationship between the flow topology and turbulence distribution. They clearly distinguished vorticity saddles and streamline saddles. Measurements were reported of two components of velocity in the wake for Reynolds numbers of the SC such as 1340, 4990 and 9980 for various inclinations such as 0, 22.5, 30, 45, and 60 by using smoke visualization and a hot-wire anemometer [7,8]. Vortex-shedding frequencies and surface pressures of the SC and rectangular cylinders in a wind tunnel were investigated experimentally using hot-film measurement techniques [9,10]. They determined the dominant peak location of the vortex shedding frequency and obtained Strouhal numbers in the range of various Reynolds numbers for the CC, SC and oriented square cylinder (OSC). The various aspects of the quasi two-dimensional (2-D) and three-dimensional (3-D) structures of the shear layer vortices, as well as the correlation of their frequency with Reynolds number for the SC, were also given by Roshko [11].

Ozgoren [12] focused on the generation of vertical structures of the near-wake region arising from flow passing the circular cylinder, square cylinder and oriented square cylinder for $550 \leq \mathrm{Re} \leq 3400$ in order to explain the physical mechanisms of the flow structure. He had supported the previous works by providing detailed quantitative experimental information with DPIV in the near- wake region of the circular cylinder and square cylinder. Ozgoren found that the values of Strouhal number, as well as the wake patterns, are functions of the cross-section of the cylinders and Reynolds numbers. Strouhal numbers for the circular cylinder, square cylinder and oriented square cylinder are found around 0.21, 0.13, and 0.17, respectively.

The purpose of this study is to investigate the effects of different angels of attacks of a square cylinder with aspect ratio of 1 at the Reynolds number of 3400 in terms of root mean square (rms) velocity and time-averaged velocity, streamline topology, and Reynolds stress correlations along with root mean square (rms) velocity. Also, Strouhal numbers and vortex formation length are calculated for the sake of comparison.

2. GOVERNING EQUATIONS

All the flow equations are presented in Cartesian tensor notation.

For unsteady incompressible flow, the conservation laws of mass, momentum and energy may be written as:

2.1. CONTINUITY

$$\frac{\partial U_i}{\partial x_i} = 0 \tag{1}$$

2.2. MOMENTUM

$$\frac{\partial(\rho U_i)}{\partial t}+\frac{\partial\left(\rho U_j U_i\right)}{\partial x_j}=-\frac{\partial P}{\partial x_i}+\frac{\partial}{\partial x_j}\left(\mu\frac{\partial U_i}{\partial x_j}-\rho\overline{u_i u_j}\right)=0 \tag{2}$$

2.3. TURBULENCE MODEL EQUATIONS

2.3.1. Standard k–e model

One of the turbulence models employed for computation is standard $k-\varepsilon$ model. In this turbulence model the Reynolds stresses are obtained via the eddy-viscosity approximation and the turbulent viscosity, ν_t, is obtained from

$$\mu_t=\rho C_\mu\sqrt{kL}=\rho C_\mu\frac{k^2}{\varepsilon} \tag{3}$$

The transport equations for k and ε are written as

$$\frac{\partial(\rho\ k)}{\partial t}+\frac{\partial(\rho\ \overline{u}_i k)}{\partial x_i}=-\frac{\partial}{\partial x_i}\left(u_i\left(\overline{\frac{u_j u_j}{2}+\frac{p}{\rho}}\right)\right)-\rho\ \overline{u_i' u_j'}\frac{\partial\overline{u}_i}{\partial x_j}+\mu\ \frac{\partial^2 k}{\partial x_i\partial x_j}-2\mu\ \frac{\overline{\partial u_j'}}{\partial x_i}\frac{\overline{\partial u_j'}}{\partial x_i} \tag{4}$$

$$\frac{\partial(\rho\varepsilon)}{\partial t}+\frac{\partial(\rho u_j\varepsilon)}{\partial x_i}=C_{\varepsilon 1}P_k\frac{\varepsilon}{k}-\rho C_{\varepsilon 2}\frac{\varepsilon^2}{k}+\frac{\partial}{\partial x_j}\left(\frac{\mu_t}{\sigma_\varepsilon}\frac{\partial\varepsilon}{\partial x_j}\right) \tag{5}$$

Where P_k, the generation rate of turbulent kinetic energy, is obtained from Eq.(7)

$$P_k=-\rho\overline{u_i' u_j'}\frac{\partial\overline{u}_i}{\partial x_j}\approx\mu_t\left(\frac{\partial\overline{u}_i}{\partial x_j}+\frac{\partial\overline{u}_j}{\partial x_i}\right)\frac{\partial\overline{u}_i}{\partial x_j} \tag{6}$$

The coefficients in Eqs. (4)-(7) are given in (8)

$$C_\mu=0.09;\quad C_{\varepsilon 1}=1.44;\quad C_{\varepsilon 2}=1.92;\quad \sigma_k=1.0;\quad \sigma_\varepsilon=1.3. \tag{7}$$

The logarithmic law of the wall due to von karman is applied for the near wall treatment.

$$u^+=\frac{\overline{v}_t}{u_\tau}=\frac{1}{\kappa}\ln n^+ + B \tag{8}$$

Where is von karman coefficient. In this formula u^+ and n^+ are calculated as:

$$u_\tau=\sqrt{|\tau_w|/\rho} \tag{9}$$

$$n^+=\frac{\rho\ u_\tau n}{\mu} \tag{10}$$

$$\tau_w=\rho u_\tau^2=\rho\ C_\mu^{1/4}\ \kappa\ \sqrt{k}\ \frac{\overline{v}_t}{\ln(n^+E)} \tag{11}$$

For the first grid after solid wall (p) no slip boundary condition is applied. For this grid k is assumed to be zero but dissipation is obtained by

$$\varepsilon=\nu\left(\frac{\partial^2 k}{\partial n^2}\right)_{wall} \tag{12}$$

$$\left(\frac{\partial \overline{v}_t}{\partial n}\right)_p = \frac{u_\tau}{\kappa n_p} = \frac{C_\mu^{1/4}\sqrt{k_p}}{\kappa n_p} \tag{13}$$

$$\varepsilon_p = \frac{C_\mu^{3/4} k_p^{3/2}}{\kappa n_p} \tag{14}$$

This wall function is applied if only $n^+_p > 30$.

2.3.2. V2f model

Dissipation equation:

$$\frac{\partial(\rho\varepsilon)}{\partial t} + \frac{\partial(\rho U_j \varepsilon)}{\partial x_j} = \frac{\partial}{\partial x_j}\left(\frac{\mu_t}{\sigma_\varepsilon}\frac{\partial \varepsilon}{\partial x_j}\right) + \rho\,\frac{C_{\varepsilon 1}P_k - C_{\varepsilon 2}\varepsilon}{\tau} \tag{15}$$

$\overline{v^2}$ equation:

$$u_j \frac{\partial\left(\rho\overline{v^2}\right)}{\partial x_j} = \frac{\partial}{\partial x_j}\left(\left(\mu + \frac{\mu_t}{\sigma_k}\right)\frac{\partial \overline{v^2}}{\partial x_j}\right) - 6\rho\overline{v^2}\frac{\varepsilon}{k} + \rho k f \tag{16}$$

f equation:

$$L^2 \frac{\partial^2 (f)}{\partial x_j^{\,2}} - f = \frac{C_1}{\tau}\left(\frac{\overline{v^2}}{k} - \frac{2}{3}\right) - C_2\frac{P_k}{k} - 5\frac{\overline{v^2}}{k\tau} \tag{17}$$

Where

$$L = C_L \max\left(\frac{k^{3/2}}{\varepsilon}, C_\eta \frac{v^{3/4}}{\varepsilon^{1/4}}\right), \quad C_{\varepsilon 1} = 1.4\left(1 + C_{\varepsilon d}\sqrt{k/\overline{v^2}}\right) \tag{18}$$

The constants of this model are:

$$\begin{aligned} &C_\mu = 0.19;\ C_{\varepsilon d} = 0.045;\ C_{\varepsilon 2} = 1.9;\ \ C_1 = 0.4;\ C_2 = 0.3; \\ &\sigma_k = 1.0;\ \sigma_\varepsilon = 1.3;\ C_L = 0.23;\ C_\eta = 70. \end{aligned} \tag{19}$$

3. NUMERICAL METHOD AND COMPUTATIONAL DOMAIN

In the present study the transport equations are solved using finite-volume methodology in a collocated grid system. Central difference scheme is employed for approximation of both convective and diffusive terms in all transport equations. A third order Runge-Kutta algorithm was used for the time integration. The pressure field is linked to that of velocity through the well-known SIMPLE pressure correction algorithm. To avoid stability problems associated with pressure-velocity decoupling the Rhio and Chow (1983) interpolation scheme is also employed.

The computation domain consists of a square cylinder obstacle of aspect ratio of one (width/height = 1) in the free stream. The domain height was selected as 8D and the spanwise width of the domain was selected as 20D such that the square is located in the middle of domain with equal distance to the spanwise boundaries. The upstream distance from the front side of the square to the inlet boundary was selected as 6D and the downstream distance was 13D. The computational domain is depicted in fig. 1.

The boundary conditions used in the present calculations are as follows:

The inlet boundary condition was selected as a uniform flow and the outlet boundary condition of convective type

$$\frac{\partial u}{\partial t}+U_{in}\frac{\partial u}{\partial x}=0$$

Obviously, such boundary condition is capable of predicting unsteady flow behavior at the exit with good accuracy (Rodi et al. (1995)). The spanwise boundary condition was selected as symmetric and no-slip boundary condition was used at the wall of square.

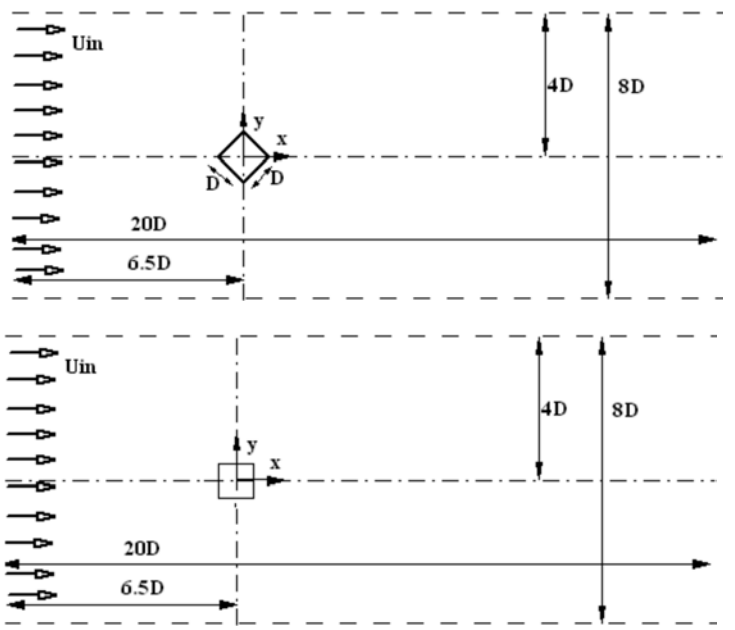

Figure 1 Computational domain for square cylinders.

4. RESULTS

In order to evaluate the influences of grid system on the results, three grid systems were used in the calculation of square cylinder with the angle of incidence of zero. The influences of these grid systems are checked for the Strouhal number and length of wake as shown in table (1). The length of wake is defined as the furthest distance along the centerline behind the cylinder in which the velocity is negative. It can be used as a measure of how far away from the cylinder the underlying potential flow has been altered by the vorticity produced. It can be seen from the table that no obvious difference on these parameters is observed between grid systems 150 × 90 and 200 × 120. So for all results presented in the present paper, the grid system consists of 150 × 90 nodes are adopted. The grid system used in this study for the case of square cylinder with the angle of incidence of $\alpha = 45°$ is shown in Fig. (2). The minimum grid spacing used in the present computation is 0.015 in all direction adjust to the square surface with grid expansion ratio of 1.02. The grid used in computations consists of (150 × 90) grid nodes in the stream-wise (x) and cross-stream (y) directions respectively. In this study Reynolds number was selected 3400.

Table 1 Grid independency for square cylinder with $\alpha = 0°$ at free stream and *Re = 3400*

L/D	St	Number of grid points
0.65	0.143	120 × 60
0.7	0.144	150 × 90
0.72	0.144	200 × 120
0.81	0.139	120 × 60
0.9	0.137	150 × 90
0.915	0.137	200 × 120

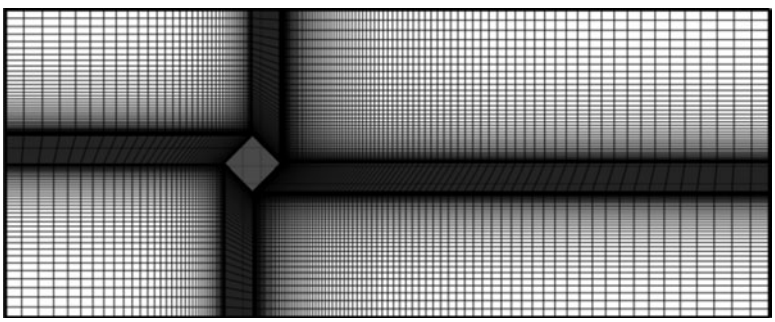

Figure 2.1 Grid system in the full computational domain at $\alpha = 45°$.

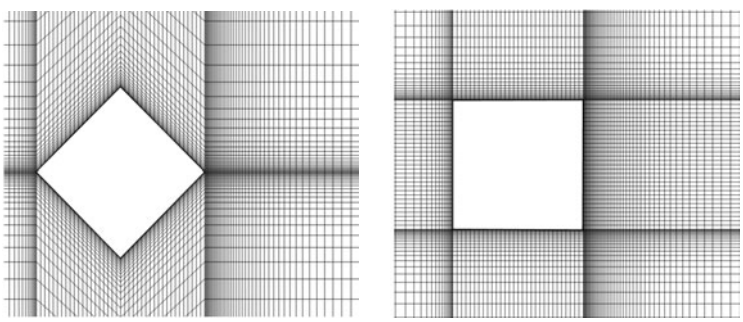

Figure 2.2 Grid system used just around the square cylinder at $\alpha = 0°, 45°$.

To validate our work a comparison between results obtained in this study and experimental results of Ozgoren [12] is done. In table (2) flow parameters such as Strouhal number and the length of wake are presented. This table clearly indicates that the present results are in good agreement with the pervious experimental results for two cases of cylinders with $\alpha = 0°, 45°$. On the other hand results obtained with $\overline{v^2} - f$ model are closer to experimental data and $\overline{v^2} - f$ model leads to more accurate data.

Table 2 A comparison between results of present study and experimental data

Strouhal number (St)			length of wake (L/D)			geometry
Experiment	$\overline{v^2} - f$	$k - \varepsilon$	Experiment	$\overline{v^2} - f$	$k - \varepsilon$	
0.13	0.137	0.144	1.2	0.9	0.7	Square cylinder $\alpha = 0°$
0.165	0.16	0.155	2.2	2.0	2.8	Square cylinder $\alpha = 45°$

Drag coefficient on the surface of cylinder is presented in table (3). This coefficient is obtained according to the dimension of cylinder, D, and free stream velocity. The data in the table reveals that with increasing angle of incidence from $\alpha = 0°$ to $\alpha = 45°$, drag coefficient on the cylinder will increase by both turbulence models. This is the fact that should be regarded in the practical applications.

Table 3 Comparison of calculated drag coefficient for $\alpha = 0°$, 45° by turbulence models

	$k-\varepsilon,\ \alpha = 0°$	$\overline{v^2}-f,\ \alpha = 0°$	$k-\varepsilon,\ \alpha = 45°$	$\overline{v^2}-f,\ \alpha = 45°$
Drag coefficient	1.4961	1.1764	1.5411	1.9966

The effect of the angle of incidence and turbulence models on the time-averaged streamlines at *Re = 3400* was investigated and results are shown in Fig. (3). The shape of vortex contours in the near-wake is similar for both geometries. Comparison of the time-averaged streamline topology with each other shows that flow structures of the wake are almost equally symmetrical with respect to the centerline of the cylinders with both angels of incidences and turbulence models for *Re = 3400.* When increasing the angle of incidence at Re = 3400 it is worth mentioning some features in the region at the downstream part of the body. The changes in the length and width of wake could be seen clearly from this figure. There is an increase in the length of wake from $\alpha = 0°$ to $\alpha = 45°$. As can be seen from the figure results obtained by $\overline{v^2}-f$ model are much more accurate.

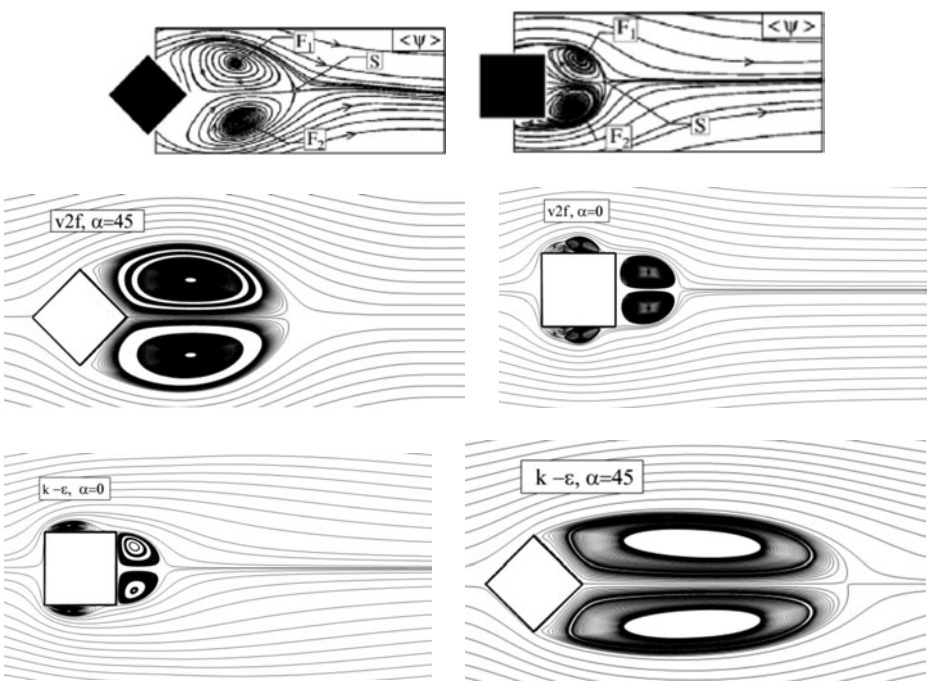

Figure 3 Comparison of time averaged streamlines with the experimental results.

The results on the distributions of mean stream-wise non-dimensional velocity is presented in Fig .4. In this figure negative quantities are displayed with dashed lines and solid lines display positive quantities. According to this kind of presentation the saddle point, where dashed lines finish and solid lines start, could be clearly seen. Results obtained by $\overline{v^2}-f$ and $k-\varepsilon$ model are compared by experimental results. It is obvious that $\overline{v^2}-f$ model can predict the location of saddle point in the downstream of square cylinder at $\alpha = 45°$ accurately.

The non dimensional root mean square velocity in the streamwise direction is computed by $k-\varepsilon$ and $\overline{v^2}-f$ models in different cross sections of computational domain at the downstream part of the body (x/D = 0.25, 0.75, 1.5, 2.5) and results are shown in Fig. (5). In the downstream of cylinder, in the closer sections to the cylinder such as x/D = 0.25, 0.75 the root mean square velocity predicted by $\overline{v^2}-f$ model is more than $k-\varepsilon$ model. On the other hand in the sections far away from the cylinder such as and x/D = 1.5 and x/D = 2.5 the root mean square velocity predicted by $\overline{v^2}-f$ model is less than $k-\varepsilon$ model which valid our results in table (2).

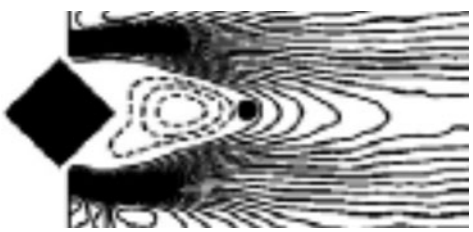

Experimental data [12]

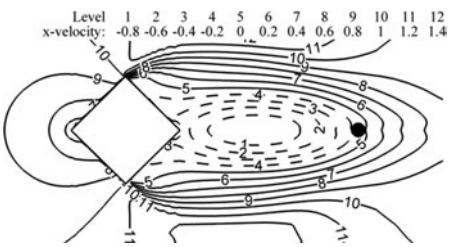

$v2f$

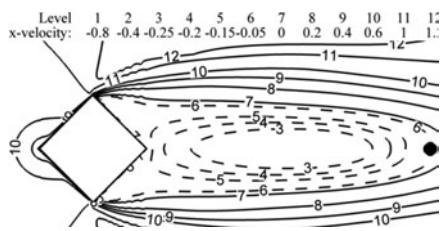

$k-\varepsilon$

Figure 4 Time averaged non dimensional stream-wise velocity contours for α = 45°.

A comparison of the variation of non dimensional time averaged streamwise velocity in the centerline of the channel along the stream direction at the downstream part of the body is made in Fig. 6. One of the benefits of this diagram is computing the location of saddle point in the downstream for $\alpha = 0º, 45º$. It is clear that the length of recirculation zone in the downstream of cylinder for $\alpha = 0º$ is predicted approximately the same by both turbulence models.

5. CONCLUSIONS

The effects of angle of incidence on turbulent flow over square cylinder in free stream at Reynolds number of 3400 were numerically investigated using URANS model two different turbulence models, $v2f$ and standard $k-\varepsilon$. Studies were carried out for angle of incidence $\alpha = 0º$ and $\alpha = 45º$. Flow parameters such as Strouhal number and drag coefficient and length

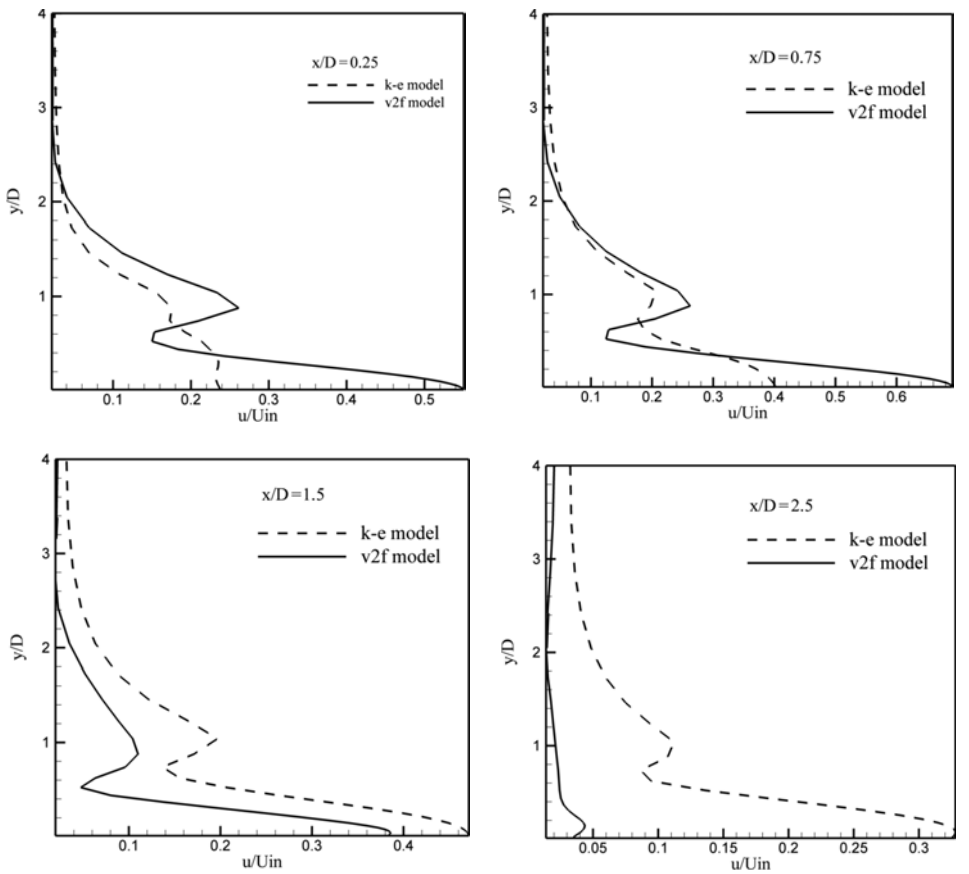

Figure 5 The non dimensional root mean square velocity in the streamwise direction in different sections for the case of $\alpha = 45°$.

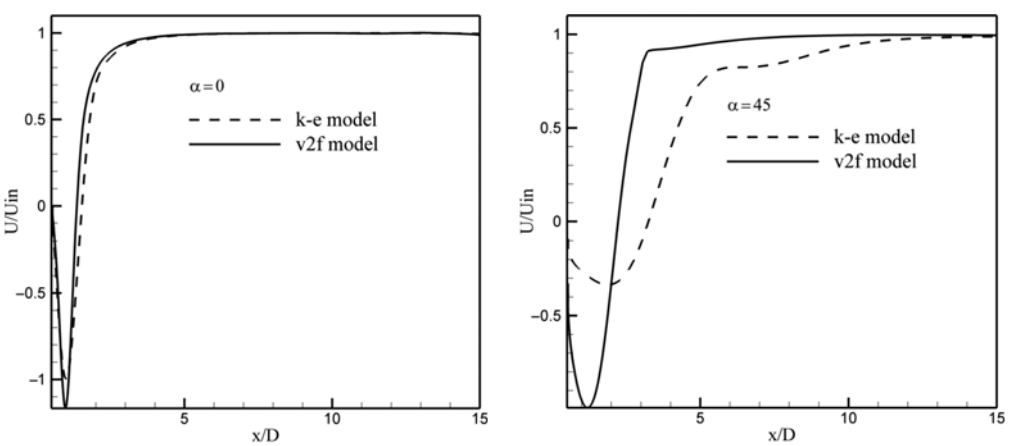

Figure 6 Comparison of time averaged streamwise velocity by two turbulence models.

of wake were presented for the case of angle of incidence $\alpha = 0^{o}$, $\alpha = 45^{o}$ with two turbulent models. Strouhal number and the length of the wake are larger for the case of $\alpha = 45^{o}$ because of the sharp corners in it which results in more diffusion of turbulence in the downstream of the cylinder. On the other hand, with comparison of results obtained by $v2f$ and standard $k-\varepsilon$ models with experiment, it is obvious that $v2f$ leads to much more accurate results.

REFRENCES

[1] C.H.K. Williamson, *Vortex dynamics in a cylinder wake*, Annual Review of Fluid Mechanic, 1996, 28, 477–539.

[2] E. Naudaschser, D. Rockwell, *Flow-induced vibrations: an engineering guide*, 1994, Rotterdam: A. A. Balkema Press.

[3] A. Okajima, Strouhal numbers of rectangular cylinders, *Journal of Fluid Mechanic*, 1982, 123, 379–98.

[4] E.D. Obasaju, An investigation of the effects of incidence on the flow around a square section cylinder, *Aeronaut Q*, 1983, 34, 243–59.

[5] D.F.G. Durao, M.V. Heitor, J.C.F. Pereira, Measurements of turbulent and periodic flows around a square cross-section cylinder, *Exp Fluids*, 1988, 6, 298–304.

[6] D.A. Lyn, S. Einav, W. Rodi, J.H. Park, A laser-Doppler velocimetry study of ensemble-averaged characteristics of turbulent near-wake of a square cylinder, *Journal of Fluid Mechanic*, 1995, 304, 285–319.

[7] A.K. Saha, K. Muralidhar, G. Biswas, Experimental study of flow past a square cylinder at high Reynolds numbers, *Exp Fluids*, 2000, 29, 553–63.

[8] S. Dutta, K. Muralidhar, P.K. Panigrahi, Influence of the orientation of a square cylinder on the wake properties, *Exp Fluids*, 2003, 34, 16–23.

[9] J.M. Chen, CH. Liu, Vortex shedding and surface pressures on a square cylinder at incidence to a uniform air stream, *International Journal of Heat and Fluid Flow*, 1999, 20, 592–7.

[10] M. Sarioglu, T. Yavuz, *Subcritical flow around bluff bodies*, AIAA Journal, 2002, 40(7), 1257–68.

[11] A.J. Roshko, Perspectives on bluff-body aerodynamics, *J Wind Eng Ind Aero*, 1999, 49, 79–100.

[12] M. Ozgoren, Flow structure in the downstream of square and circular cylinders, *Flow Measurement and Instrumentation*, 2006, 17, 225–235.